Efficient channel coding for multipulse pulse position modulation in terrestrial FSO systems

Fang Xu, Mohammad-Ali Khalighi, Salah Bourennane

École Centrale Marseille, Institut Fresnel, Marseille, France

ABSTRACT

For terrestrial free space optical (FSO) systems, we investigate the use of multipulse pulse position modulation (MPPM), which has the advantage of bandwidth efficiency compared to the classical PPM. We first discuss the upper-bound on the information transmission rate for the case of a Gaussian (turbulence-free) channel. We next consider the channel coding issue for MPPM. We propose to use a simple binary convolutional code and to perform iterative soft demodulation and channel decoding at the receiver. We study the performance of this scheme by presenting some numerical results for the cases of Gaussian and weak-turbulence channels. We also show that, in contrast to PPM, the bit-symbol mapping is an important point for MPPM, especially regarding the proposed iterative receiver. In this view, we propose design rules for optimal bit-symbol mapping.

Keywords: Free space optics, atmospheric turbulence, multi-pulse pulse position modulation, channel coding, iterative detection

1. INTRODUCTION

Free Space Optics (FSO) or optical wireless communication is a promising solution for the need to very high data rate point-to-point communication.[1] In practice, several factors such as pointing errors, beam dispersion, atmospheric absorption and propagation loss associated with visibility can degrade the performance of an FSO system. We assume in this paper clear atmosphere conditions and perfect alignment of transmitter and receiver. Under these conditions, the system performance can still be affected by atmospheric turbulence that causes random fluctuations in both the amplitude and the phase of the received signal; what is called channel fading.[2]

Under weak turbulence conditions, channel coding is an efficient solution for improving the link performance.[3,4] The system performance can be further improved by using efficient modulation techniques. We have considered in a recent work the use of the pulse position modulation (PPM) and proposed the use of a simple binary convolutional code for channel coding.[5] The interest of PPM is that it is average-energy efficient. At the receiver, we proposed to use an iterative soft demodulation and decoding scheme, called BCID (standing for Binary Convolutional encoding with Iterative Detection) to improve the system performance. The interest of such a scheme is that, for the case of non-binary PPM, it can efficiently correct the demodulator errors without employing a non-binary code necessitating computationally complex decoding at the receiver. By the iterative scheme, the signal demodulation can benefit from the channel coding gain to correct demodulation errors, at the same time, the receiver complexity remains reasonable.

We consider in this paper the case of multipulse PPM (MPPM), which compared to PPM, has the advantage of reduced peak-to-average power ratio (PAPR) and higher bandwidth efficiency. We extend the BCID scheme to MPPM. We show that, in contrast to PPM, the bit-symbol mapping is an important point for MPPM, especially regarding the proposed iterative receiver. In this view, we propose design rules for optimal bit-symbol mapping. We first study the impact of bit-symbol mapping on the channel capacity in the absence of turbulence. Then, we discuss its effect on the performance of the iterative receiver. We also provide a design rule for optimal bit-symbol mapping for MPPM.

Note that we use interchangeably the terms of demodulation (demodulator) and demapping (demapper). We assume that we do not have any source of diversity available. This assumption of the absence of any source

Further author information: (Send correspondence to Fang XU)
Fang XU: Email: Fang.Xu@fresnel.fr, Phone: (+33) 491288202

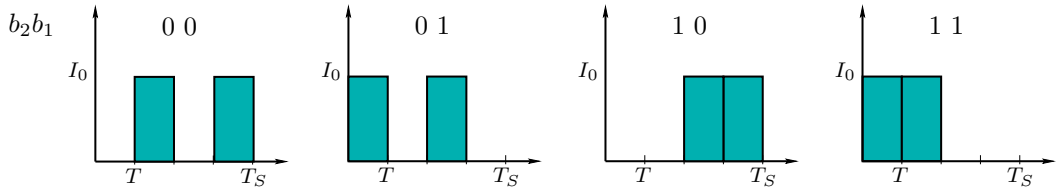

Figure 1. Mapping Example for 2-4PPM symbols. I_0 stands for the transmitted light intensity in an ON slot.

of diversity allows us to focus on the performance of MPPM. For the performance analysis of the receiver, we consider two cases of absence of turbulence and a weak-turbulence channel. Note that this latter case is not restrictive, because it is equivalent to the case of moderate or strong turbulence when a relatively large lens is used at the receiver for aperture averaging.[2,6]

The remainder of this paper is organized as follows. In Section 2, we present our system model and general assumptions. Next, we present a brief state of the art on MPPM in Section 3. Also, the information transmission bounds are studied for a non-random MPPM channel, i.e., in the absence of turbulence. We briefly review the iterative detection, including MPPM bit-symbol mapping and soft demodulation in Section 4. In Section 5, we discuss the optimal bit-symbol mapping for MPPM. Some numerical results are presented in Section 6, and Section 7 concludes the paper.

2. SYSTEM MODEL AND ASSUMPTIONS

At the transmitter, the information bits are first encoded with a classical binary convolutional code. Then the interleaved encoded bits are transformed into symbols according to the MPPM modulation. Pseudo-random interleaving is considered. We denote by I_0 the transmitted light intensity in an ON MPPM slot. We consider the Gamma-Gamma ($\Gamma\Gamma$) statistical model for the channel fades.[2] Also, we consider frozen channel model for the channel time variations. That is to say, channel fading coefficient h remains constant over the duration of a frame of symbols, and changes to a new independent value from one frame to next.

At the receiver, we denote by I, the received intensity corresponding to I_0 in an ON MPPM slot. In fact, we have $I = hI_0$. After optical/electrical conversion, the received signal r is:

$$r = \eta\, h\, I_0 + n, \tag{1}$$

where η is the optical/electrical conversion efficiency assumed here to be unity for simplicity. Also, n is the receiver noise, assumed to be dominated by thermal noise, and modelled by a zero-mean Gaussian additive random process. Note that for an OFF MPPM slot, we have $r = n$.

We perform soft demodulation on the received signal r based on the maximum *a posteriori* (MAP) criterion, followed by soft channel decoding. Soft information at the demodulator or decoder output is considered in the form of logarithmic likelihood ratio (LLR). We assume that perfect time synchronization is done and we do not have any inter-slot interference (ISI).

3. MULTI-PULSE PULSE POSITION MODULATION

For the classical Q-ary PPM (denoted hereafter by QPPM), a symbol duration is cut into Q time slots (or chips), and an optical pulse is sent in one of these Q slots. So it has a duty cycle of $1/Q$ and a PAPR of Q. We can vary Q to make a flexible compromise between power efficiency and bandwidth efficiency. However, with a larger Q, the PAPR increases for a given average transmission power. Also, the required switching speed for electronic circuits increases and the receiver synchronization becomes more difficult.[7]

Bandwidth efficiency is a parameter of critical importance in FSO systems. For this reason, we consider in this paper multipulse PPM (MPPM). By MPPM, we send w laser pulses among Q slots. We use the notation of w-QPPM for which we have a duty cycle of w/Q and a PAPR of Q/w. The advantage of MPPM over PPM is its reduced PAPR and its higher bandwidth efficiency.[8] We have to note that PPM still remains more average-energy efficient than MPPM. In fact, to achieve a given bit error rate (BER), the required average power by

MPPM is more than that of PPM. The comparison of the performances of PPM and MPPM has been done in several works.[8,9]

For the general case of w-QPPM, there are $C_w^Q = \binom{Q}{w}$ possibilities of choosing w "on" slots among Q. So, every MPPM symbol can represent up to $L = \log_2(C_w^Q)$ bits. However, C_w^Q may not be a power of two, so, benefiting from the maximum L may require a complicated bit-symbol mapping. For instance, it is suggested in[9] to cascade several MPPM symbols to benefit from the maximum total number of bits. In this paper, as a simple solution, we take the integer part of L as the number of bits per symbol B. However, due to this simplification, the system performance will depend on the choice of Q symbols among $P_{2^B}^{C_w^Q}$ possible bit-symbol mappings. In other words, there are $P_{2^B}^{C_w^Q}$ possibilities for mapping the bit set $\{b_B b_{B-1} ... b_1\}$ into a symbol set $\{x_1 x_2 ... x_Q\}$. Moreover, as we will explain in Section 5, different ways of bit-symbol mapping can affect considerably the performance of the iterative receiver. An example of bit-symbol mapping for the case of 2-4PPM is given in Fig. 1 where we have simply taken $B = 2$ bits, whereas $L = 2.58$.

3.1 Channel capacity

It is interesting to compare the upper bounds on the information transmission rate for PPM and MPPM modulations. Although these bounds cannot really be called *capacity* in the sense of Shannon (because of restricting the distribution of the transmitted signal according to the underlying modulation), for simplicity we will call them capacity of PPM or MPPM.

The capacity of PPM and MPPM channels has been studied in several works[8,10,11] for the case of deep-space communication using a photon counting receiver, where the Poisson channel model is considered. We consider in this paper the case of terrestrial FSO systems used over ranges up to several kilometers. In such systems, photon counting is not feasible in practice. In fact, the received photon flux is important and we can detect the received signal based on the beam intensity directly. Here, we consider the channel capacity for different modulation schemes for intensity-based signal detection. According to the assumptions of Section 2, the receiver noise has a Gaussian distribution. On the other hand, the MPPM constellation is considered of size C_w^Q and $\log_2(C_w^Q)$ bits are transmitted per MPPM symbol.[8] Here we consider the more practical case, where as a simple solution $\lfloor \log_2(C_w^Q) \rfloor$ bits are transmitted per MPPM symbol. The channel capacity is then calculated by considering the $P_{2^B}^{C_w^Q}$ different bit-symbol mappings. As mentioned previously, taking $B = \lfloor L \rfloor$ is more appropriate for a simple and practical implementation.

The channel capacity is the maximum of the mutual information $I(X;Y)$ between the channel input X and output Y, with respect to the probability mass function of X:

$$C = \max_{P_X(x)} I(X;Y). \tag{2}$$

Let us use bold-face characters $\boldsymbol{X}$ and $\boldsymbol{Y}$ for denoting channel input and output, respectively, corresponding to a QPPM or w-QPPM symbol. Hence, a symbol $\boldsymbol{x}$ (or $\boldsymbol{y}$) corresponds to Q slot-values that we denote by x_i (or y_i), $i = 1, \cdots Q$. For each time slot value, we denote by $f_{Y_i|X_i}(y_i|x_i)$ the conditional distribution of Y_i to X_i. Variable X_i takes the values 0 or 1, corresponding to an OFF- or ON-slot, respectively. As previously mentioned, we assume the absence of ISI. The conditional distribution $f_{\boldsymbol{Y}|\boldsymbol{X}}(\boldsymbol{y}|\boldsymbol{x})$ is then,

$$f_{\boldsymbol{Y}|\boldsymbol{X}}(\boldsymbol{y}|\boldsymbol{x}) = \prod_{i=1}^{Q} f_{Y_i|X_i}(y_i|x_i) \tag{3}$$

We evaluate in the following the channel capacity for the case of an additive white Gaussian noise (AWGN) channel.[10] That is to say, we consider the absence of atmospheric turbulence and set the channel fading coefficient h in (1) to one. Then we have the conditional distributions $f_{Y_i|X_i}(y_i|x_i)$:

$$\begin{cases} p_0(y_i) \triangleq f_{Y_i|X_i}(y_i|x_i = 0) = \frac{1}{\sqrt{2\pi}\sigma} \exp\left(-\frac{y_i^2}{2\sigma^2}\right) \\ p_1(y_i) \triangleq f_{Y_i|X_i}(y_i|x_i = 1) = \frac{1}{\sqrt{2\pi}\sigma} \exp\left(-\frac{(y_i-1)^2}{2\sigma^2}\right) \end{cases} \tag{4}$$

where σ^2 is the receiver noise variance.

3.1.1 Case of PPM

We assume equiprobable symbols for PPM. Without loss of generality, let us assume that the first slot is ON and the others are OFF. We denote this symbol by $\boldsymbol{x}_1$. In addition, let us denote by $\boldsymbol{x}_k$ a PPM symbol with the kth slot ON. Then the channel capacity in (2) turns to:

$$C = \int_{\mathbb{R}^Q} f_{\boldsymbol{Y}|\boldsymbol{X}}(\boldsymbol{y}|\boldsymbol{x}_1) \log_2 \left(\frac{f_{\boldsymbol{Y}|\boldsymbol{X}}(\boldsymbol{y}|\boldsymbol{x}_1)}{\frac{1}{Q}\sum_{k=1}^{Q} f_{\boldsymbol{Y}|\boldsymbol{X}}(\boldsymbol{y}|\boldsymbol{x}_k)} \right) d\boldsymbol{y} \tag{5}$$

where, $\mathbb{R}$ is the set of real numbers, and for instance,

$$f_{\boldsymbol{Y}|\boldsymbol{X}}(\boldsymbol{y}|\boldsymbol{x}_k) = p_1(y_k) \prod_{i=1, i\neq k}^{Q} p_0(y_i) \cdot \tag{6}$$

Distributions $p_0(y)$ and $p_1(y)$ are given in (4). Instead of calculating the Q-dimensional integral in (5) numerically, which becomes computationally too complex for large Q, we use Monte Carlo simulations to evaluate C.[10]

3.1.2 Case of MPPM

For the sake of demonstration simplicity, let us first consider the case of 2-4PPM and $B = 2$. For a symbol $\boldsymbol{x}_i$, $i = 1, \cdots 4$, we have two ON-slots and two OFF-slots. Let us assume the first two slots are ON and the others OFF, denoted by $\boldsymbol{x}_1$, then we have,

$$f_{\boldsymbol{Y}|\boldsymbol{X}}(\boldsymbol{y}|\boldsymbol{x}_1) = p_1(y_1)p_1(y_2)p_0(y_3)p_0(y_4)\cdot \tag{7}$$

Then the channel capacity in (5) turns to:

$$C = \frac{1}{4}\sum_{i=1}^{4} \int_{\mathbb{R}^4} f_{\boldsymbol{Y}|\boldsymbol{X}}(\boldsymbol{y}|\boldsymbol{x}_i) \log_2 \left(\frac{f_{\boldsymbol{Y}|\boldsymbol{X}}(\boldsymbol{y}|\boldsymbol{x}_i)}{\frac{1}{4}\sum_{k=1}^{4} f_{\boldsymbol{Y}|\boldsymbol{X}}(\boldsymbol{y}|\boldsymbol{x}_k)} \right) d\boldsymbol{y} \tag{8}$$

As mentioned previously, for 2-4PPM, there are $P_4^6 = 360$ different ways for mapping the bit-set $(b_2 b_1) = \{00, 01, 10, 11\}$ into a symbol-set of size 4, among the 6 possible symbols $\{0011, 0101, 0110, 1001, 1010, 1100\}$. To avoid calculate the capacities of all these possibilities, we first sort out these possibilities into $C_4^6 = 15$ symbol-sets. Then, corresponding to each symbol-set, there are $4! = 24$ possibilities for bit-symbol mapping, which have the same average Hamming distance d, because permutations do not affect d. It can be easily verified that these 15 symbol-sets can be divided into two groups that differ in d, one with $d = 2.67$ and the other with $d = 2.33$. We use Monte Carlo simulations to evaluate C for the two groups respectively.

We have shown in Fig. 2 the capacities of 2-4PPM and 2-8PPM with different average Hamming distances d and QPPM modulations $Q = 2, 4, 8, 16$, versus the receiver electrical signal-to-noise ratio (SNR), considered in the form of E_b/N_0. Note that for 2-8PPM, we have $L = \log_2(C_2^8) \simeq 4.8$ and so, we can do the mapping by taking $B = 3$ or $B = 4$. So, we have shown the capacities of 2-8PPM with maximum and minimum d for $B = 3$ and maximum d for $B = 4$. The capacity is represented in units of bits per symbol. To set the SNR, we fix the channel bandwidth, as well as the average transmitted optical power for different modulations. Note that in a previous work,[5] we have considered PPM capacity calculation, where we had fixed the peak transmitted optical power and the slot duration for any Q. Fixing the average energy is a better criterion, however, as we do here. The capacities of on-off keying (OOK) and binary PPM (BPPM) are identical. From Fig. 2 it is seen that the capacity curve of 2-8PPM with $B = 4$ lays below that of 16PPM, but above that of 8PPM, and this latter lays above the capacity curve of 2-8PPM with $B = 3$. We also notice that interestingly, the capacity of MPPM depends on d: a larger d results in larger C. For SNR$\rightarrow \infty$ the asymptotic capacity equals B bits per symbol.

4. ITERATIVE DETECTION OF MPPM SYMBOLS

In this section, we first briefly review the BCID scheme that we have considered in a previous work[5] and then, we extend it to MPPM. We also provide an example on MPPM bit-symbol mapping and soft-demodulation. Note that BCID can be considered as a simplification of the serially concatenated pulse-position modulation (SCPPM) scheme proposed by Moision and Hamkins.[12,13] This latter is more suitable for applications with relatively low data rates in the order of Mbps, such as deep space communication.

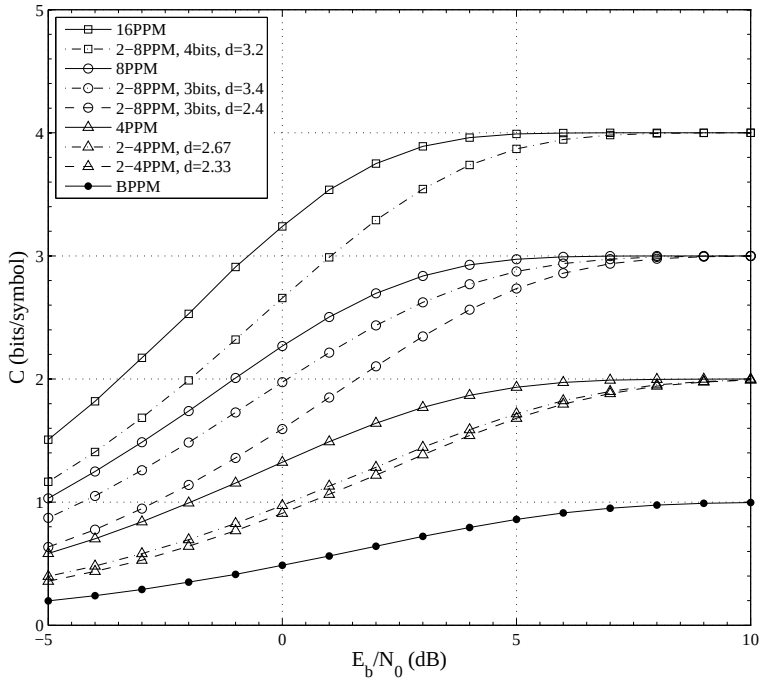

Figure 2. Capacity in units of bits per slot versus SNR for QPPM, 2-4PPM, 2-8PPM and OOK, $Q = 2, 4, 8, 16$.

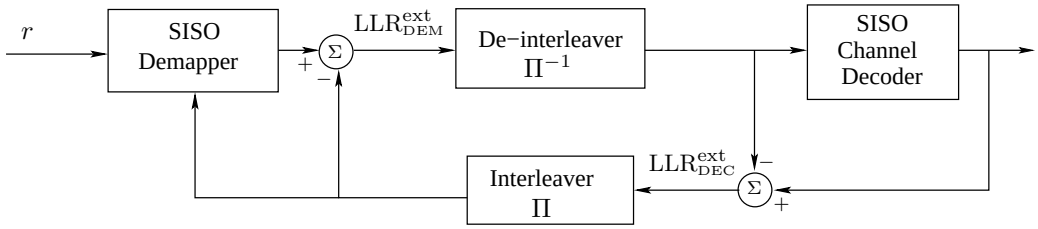

Figure 3. Block diagram of the iterative receiver. $\mathrm{LLR}^{\mathrm{ext}}_{\mathrm{DEM}}$ and $\mathrm{LLR}^{\mathrm{ext}}_{\mathrm{DEC}}$ denote the extrinsic soft-values at the demapper and the channel decoder, respectively.

4.1 Iterative demodulation and decoding

As explained previously, we use a classical binary convolutional code in the BCID scheme. The block diagram of the receiver is shown in Fig. 3. In order to improve the receiver performance, we perform soft-input soft-output (SISO) demodulation and channel decoding iteratively. The former is based on the maximum *a posteriori* (MAP) criterion, and the latter on maximum likelihood (ML) using soft-output Viterbi algorithm (SOVA).

At the first iteration, the demapper calculates bit-level LLRs on the transmitted (coded) bits using the received signal samples r. The demapper output LLRs are then fed to the SISO decoder that provides at its output LLRs on the coded bits. In the second iteration, the decoder output *extrinsic* LLRs are fed to the demodulator to help it refine the LLR calculation. The demodulator then provides the extrinsic LLRs to the decoder, and so on. After a few iterations, we practically attain the convergence. Decision making on the transmitted bits can then be done using the *a posteriori* LLRs at the decoder output. The de-interleaver in Fig. 3 has the task of decorrelating the demapper outputs to preserve the performance of the ML channel

decoder. Note that, equivalently, at the transmitter, the encoded bits are first interleaved prior to modulation. As mentioned previously, we consider pseudo-random interleaving of large enough size.

4.2 Soft demapping of MPPM symbols

Let us consider the example of 2-4PPM bit-symbol mapping illustrated in Fig. 1, for which the average Hamming distance is maximal, $d = 2.67$. At the transmitter, each block of 2 interleaved coded bits is mapped into a MPPM symbol of 4 slots: $\boldsymbol{x} = (x_1, x_2, ..., x_4)$. We refer to $\boldsymbol{x}$ as a *slot-word*. According to the Fig. 1, we have $\boldsymbol{x} = (x_1 = 0, x_2 = 1, x_3 = 0, x_4 = 1)$ for $b_2 = 0$ and $b_1 = 0$, $\boldsymbol{x} = (x_1 = 1, x_2 = 0, x_3 = 1, x_4 = 0)$ for $b_2 = 0$ and $b_1 = 1$, $\boldsymbol{x} = (x_1 = 0, x_2 = 0, x_3 = 1, x_4 = 1)$ for $b_2 = 1$ and $b_1 = 0$, and $\boldsymbol{x} = (x_1 = 1, x_2 = 1, x_3 = 0, x_4 = 0)$ for $b_2 = 1$ and $b_1 = 1$.

As explained in Subsection 4.1, here we perform MAP-based soft demodulation. According to (1), at the receiver, corresponding to a slot-word $\boldsymbol{x}$, we receive $\boldsymbol{r} = (r_1, r_2, ..., r_Q)$, where $r_i = x_i\ I + n,\ i = 1, ..., Q$. x_i equals 0 or 1, depending on the mapped MPPM symbol. Signals r_i are statistically independent according to the assumptions of Section 2. For the sake of demonstration simplicity, let us consider the case of 2-4PPM in Fig. 1. Remember the bit-symbol mapping has been illustrated previously. The likelihood ratio (LR) on the bit b_1 is given by:

$$\begin{aligned} \mathrm{LR}(b_1) &= \frac{P(\boldsymbol{r}|b_1=1)}{P(\boldsymbol{r}|b_1=0)} = \frac{P(\boldsymbol{r}|b_1=1,b_2=0)+P(\boldsymbol{r}|b_1=1,b_2=1)}{P(\boldsymbol{r}|b_1=0,b_2=0)+P(\boldsymbol{r}|b_1=0,b_2=1)} \\ &= \frac{P(\boldsymbol{r}|x_1=x_3=1,x_2=x_4=0)+P(\boldsymbol{r}|x_1=x_2=1,x_3=x_4=0)}{P(\boldsymbol{r}|x_2=x_4=1,x_1=x_3=0)+P(\boldsymbol{r}|x_3=x_4=1,x_1=x_2=0)} \end{aligned} \tag{9}$$

where, for instance, $P(\boldsymbol{r}|b_1 = 1)$ is the PDF of $\boldsymbol{r}$ conditioned to $b_1 = 1$. Taking into account our iterative detection scheme, we should also make use of the *a priori* information at the demapper input. Let us denote by L_1 and L_2 the *a priori* LLRs on the bits b_1 and b_2, respectively. These are, in fact, the extrinsic LLRs at the decoder output, calculated in the previous iteration. (Obviously, at the first iteration, these *a priori* LLRs are set to zero.) Lets use the superscripts $.^{\mathrm{apost}}$ and $.^{\mathrm{ext}}$ to explicitly denote the *a posteriori* and extrinsic soft values, respectively. We have:

$$\begin{aligned} \mathrm{LR}^{\mathrm{apost}}(b_1) &= \frac{\exp\left(\frac{-(r_1-I)^2}{2\,\sigma_n^2}+\frac{-r_2^2}{2\,\sigma_n^2}+\frac{-(r_3-I)^2}{2\,\sigma_n^2}+\frac{-r_4^2}{2\,\sigma_n^2}\right)e^{L_1}+\exp\left(\frac{-(r_1-I)^2}{2\,\sigma_n^2}+\frac{-(r_2-I)^2}{2\,\sigma_n^2}+\frac{-r_3^2}{2\,\sigma_n^2}+\frac{-r_4^2}{2\,\sigma_n^2}\right)e^{L_1+L_2}}{\exp\left(\frac{-r_1^2}{2\,\sigma_n^2}+\frac{-(r_2-I)^2}{2\,\sigma_n^2}+\frac{-r_3^2}{2\,\sigma_n^2}+\frac{-(r_4-I)^2}{2\,\sigma_n^2}\right)+\exp\left(\frac{-r_1^2}{2\,\sigma_n^2}+\frac{-r_2^2}{2\,\sigma_n^2}+\frac{-(r_3-I)^2}{2\,\sigma_n^2}+\frac{-(r_4-I)^2}{2\,\sigma_n^2}\right)e^{L_2}} \\ &= \frac{\exp\left(\frac{(r_1+r_3)I}{\sigma_n^2}\right)e^{L_1}\ +\ \exp\left(\frac{(r_1+r_2)I}{\sigma_n^2}\right)e^{(L_1+L_2)}}{\exp\left(\frac{(r_2+r_4)I}{\sigma_n^2}\right)\ +\ \exp\left(\frac{(r_3+r_4)I}{\sigma_n^2}\right)e^{L_2}} \end{aligned} \tag{10}$$

The LLR on b_1 is obtained by taking the logarithm of (10). We use the approximation of $\log(e^m+e^n) \approx \max(m, n)$ to simplify the calculation of LLRs. Then, (10) simplifies to:

$$\mathrm{LLR}^{\mathrm{apost}}(b_1) \approx \max\left(\frac{(r_1+r_3)I}{\sigma_n^2}+L_1\ ,\ \frac{(r_1+r_2)I}{\sigma_n^2}+L_1+L_2\right)-\max\left(\frac{(r_2+r_4)I}{\sigma_n^2},\frac{(r_3+r_4)I}{\sigma_n^2}+L_2\right). \tag{11}$$

Remember that we have to provide extrinsic LLRs for the SISO decoder. Then,

$$\mathrm{LLR}^{\mathrm{ext}}(b_1) = \mathrm{LLR}^{\mathrm{apost}}(b_1) - L_1 = \max\left(\frac{(r_1+r_3)I}{\sigma_n^2},\frac{(r_1+r_2)I}{\sigma_n^2}+L_2\right)-\max\left(\frac{(r_2+r_4)I}{\sigma_n^2},\frac{(r_3+r_4)I}{\sigma_n^2}+L_2\right). \tag{12}$$

Similarly, the extrinsic LLR on b_2 is calculated as follows.

$$\mathrm{LLR}^{\mathrm{ext}}(b_2) = \max\left(\frac{(r_3+r_4)I}{\sigma_n^2},\frac{(r_1+r_2)I}{\sigma_n^2}+L_1\right)-\max\left(\frac{(r_2+r_4)I}{\sigma_n^2},\frac{(r_1+r_3)I}{\sigma_n^2}+L_1\right) \tag{13}$$

Checking (12) and (13), we see that the extrinsic LLR on a bit does not depend on its *a priori* LLR.

5. OPTIMAL MPPM BIT-SYMBOL MAPPING FOR ITERATIVE SCHEME

As a matter of fact, the performance of iterative scheme does not depend only on d and other criteria should be taken into account. To show clearly that d is not the only parameter affecting the iterative receiver performance, let us look at another example of 2-4PPM bit-symbol mapping, still with the maximum $d = 2.67$. The bit-symbol mapping is done as follows: $\boldsymbol{x} = (x_1 = 0, x_2 = 1, x_3 = 0, x_4 = 1)$ for $b_2 = 0$ and $b_1 = 0$, $\boldsymbol{x} = (x_1 = 0, x_2 = 1, x_3 = 1, x_4 = 0)$ for $b_2 = 0$ and $b_1 = 1$, $\boldsymbol{x} = (x_1 = 1, x_2 = 0, x_3 = 0, x_4 = 1)$ for $b_2 = 1$ and $b_1 = 0$, and $\boldsymbol{x} = (x_1 = 1, x_2 = 0, x_3 = 1, x_4 = 0)$ for $b_2 = 1$ and $b_1 = 1$. For soft demapping at the receiver, we calculate the extrinsic LLR on b_1 and b_2 by taking the same procedure explained in previous section. For instance, the extrinsic LLR on b_1 is:

$$\mathrm{LLR}^{\mathrm{ext}}(b_1) = \max\left(\frac{(r_2 + r_3)I}{\sigma_n^2}, \frac{(r_1 + r_3)I}{\sigma_n^2} + L_2\right) - \max\left(\frac{(r_2 + r_4)I}{\sigma_n^2}, \frac{(r_1 + r_4)I}{\sigma_n^2} + L_2\right) = \frac{(r_3 - r_4)I}{\sigma_n^2}. \quad (14)$$

We notice that for this bit-symbol mapping, $\mathrm{LLR}^{\mathrm{ext}}(b_1)$ only depends on the received signals and the *a priori* information on b_2 does not help the detection of b_1. In other words, this mapping does not work in the iterative scheme, although it has the maximum d.

Note that the example of bit-symbol mapping that we considered in the previous section (Fig. 1) is an optimal one. We discuss a general guideline for appropriate bit-symbol mapping for 2-4PPM in the following.

5.1 Mapping guidelines for 2-4PPM

Here, we provide details on the optimal bit-symbol mapping by considering the example of 2-4PPM. We have explained in Section 3 that for 2-4PPM, we have sorted out 360 different ways of bit-symbol mapping into two groupes of symbol-sets that differ in d. As we saw in the above example, the performance of the iterative scheme depends not only on d and we should further optimize the mapping. For this purpose, corresponding to a special symbol-set, we furthermore specify the parameters d_1 and d_2, which are the average Hamming distances between two symbols (slot-words) differing in one and two bits in $(b_2 b_1)$, respectively. We have resumed in Table 1 the classification of different mappings, where we have specified d, d_1, and d_2 for different symbol-sets together with the number of mapping ways corresponding to each set. We have also provided a mapping example at the right of each set in Table 1. The first one, i.e.,"Unacceptable," is what we illustrated in the first part of this section. And the second one, i.e.,"Best," is what we had already illustrated in Fig. 1.

Table 1. Possible bit-symbol mappings and examples for 2-4PPM

Number of symbol-sets	Number of possible bit-symbol mappings	d	d_1	d_2	$b_2 b_1$	0 0	0 1	1 0	1 1
3	$8 \times 3 = 24$	2.67	2	4	Unacceptable	0 1 0 1	0 1 1 0	1 0 0 1	1 0 1 0
3	$16 \times 3 = 48$	2.67	3	2	Best	0 1 0 1	1 0 1 0	0 0 1 1	1 1 0 0
12	$8 \times 12 = 96$	2.33	2	3	Bad	0 1 0 1	0 0 1 1	1 1 0 0	0 1 1 0
12	$16 \times 12 = 192$	2.33	2.5	2	Good	0 0 1 1	0 1 0 1	1 1 0 0	0 1 1 0

The distances d, d_1, and d_2 are important parameters that affect the receiver performance. The most important parameter is d: a larger d results in general in a lower symbol error rate. The BER on the other hand, depends also on d_1 and d_2. In the case of non-iterative detection, the more important parameter after d is d_2: To obtain a better performance, we should first choose a mapping with the largest d, and then maximize in descending priority order, d_2 and d_1. If we perform iterative detection, however, to optimize the mapping, after maximizing d, we should maximize in descending priority order, d_1 and d_2. This concept is similar to the so called *Anti-Gray* mapping, already investigated for RF communication systems employing iterative detection.[14,15] In particular, S. ten Brink studied for different mappings, the bit-wise mutual information (MI) on a bit, given the *a priori* knowledge of one or more bits.[14] He showed that for a better performance improvement through iterations, this conditioned bit-wise MI should be maximized. The Anti-Gray mapping and the mapping method we proposed above satisfy this criterion.

From Table 1, the mapping that we called "Best" is optimized following this guideline. The performance comparison of the four mapping examples will be done in Subsection 6.3. Note that for the classical Q-ary PPM, we have $d = d_1 = d_2 = \cdots = 2$ irrespective of the mapping. So, we have the same convergence property for any mapping.

6. NUMERICAL RESULTS

Here we present some simulation results to study the performance of BCID scheme with MPPM modulation. The system performance is evaluated in terms of average BER as a function of E_b/N_0.

6.1 Simulation parameters

For channel coding, we consider the rate 1/2 recursive systematic convolutional (RSC) code $(1, 5/7)$ of constraint length $K = 3$, where the numbers 5 and 7 represent the code polynomial generators in octal. Also, we consider two cases of AWGN channel, i.e., without atmospheric turbulence, and weak-turbulence channel. For the latter case, we set the Rytov variance to $\chi^2 = 0.04$. Normalized channel is considered, i.e., $\mathrm{E}\{I\} = 1$.

6.2 Performance of different modulations

Let us begin by comparing the performances of PPM modulation and MPPM modulation. For the sake of completeness, we also consider the case of OOK modulation.

To do a fair comparison between the performances of different modulations, we fix for all modulation schemes the *information* transmission rate that we denote by R, as well as the average transmitted *optical* power, denoted by P_{av}. Fixing this latter parameter is important because it controls the total optical energy consumption for the transmission of a given volume of data. On the other hand, as we consider RSC coding with coding rate $R_c = 1/2$, the (encoded data) bit rate R_b equals R/R_c. Since for all modulations, channel coding and R_c are the same, fixing R turns to fixing R_b.

Taking fixed R_b and P_{av} into account, we set the transmitted beam intensity I_0 (in ON slots) for a given modulation. Considering the noise unilateral power spectral density N_0, we also have to set the receiver noise variance σ_n^2 according to the occupied bandwidth that we consider as $1/T$, where T is the slot duration. We specify below the calculation of I_0, σ_n^2, and E_b for different modulations that we will consider. Notice that we take R_c into account in the calculation of E_b.

- For OOK modulation, we have $T = T_s = 1/R$ and hence we set: $I_0 = 2\ P_{av}$; $\sigma_n^2 = \frac{N_0}{2} R$; $E_b = \frac{2\ {P_{av}}^2}{R_b}$.
- For QPPM, we have $T = T_s/Q = \frac{\log_2 Q}{Q\,R}$. We set: $I_0 = Q\ P_{av}$; $\sigma_n^2 = \frac{N_0}{2} \frac{Q}{\log_2 Q} R$; $E_b = \frac{Q\ {P_{av}}^2}{R_b}$.
- For w-QPPM, with B bits per symbol, we have $T = T_s/Q = \frac{B}{Q\,R}$. Then, we set $I_0 = \frac{Q\ P_{av}}{w}$; $\sigma_n^2 = \frac{N_0}{2} \frac{Q}{B} R$; $E_b = \frac{Q\ {P_{av}}^2}{w\ R_b}$.

6.2.1 Case of AWGN channel

Let us first consider an AWGN channel, i.e., without atmospheric turbulence. We have contrasted in Fig. 4 the BER curves versus SNR corresponding to the first, second, and fifth iterations, for the cases of 4PPM and 2-4PPM, as well as the BER curve for the case of OOK. We have set the interleaver size to about 2000, 4000, and 4000 for OOK, 4PPM, and 2-4PPM, respectively. Negligible improvement is obtained for larger interleavers.

Concerning modulation schemes, as expected, the overall performance of 2-4PPM is not better than 4PPM; even, it is worse than OOK without iterative detection. In fact, 4PPM remains more energy efficient and hence, for a given E_b/N_0, it has a lower BER than 2-4PPM. As expected, the gain obtained by the iterative method is specially considerable for 4PPM and 2-4PPM modulations. We notice that for 2-4PPM, there is a more significant gain than what we had for a simple 4PPM. For instance, at BER= 10^{-5} and after full convergence, the SNR gain by iterative detection is about 0.88 dB and 1.86 dB for the cases of 4PPM and 2-4PPM, respectively. The interesting point is that, it is sufficient to process only two iterations at high enough SNR for 4PPM. However, for 2-4PPM, we should process about five iterations.

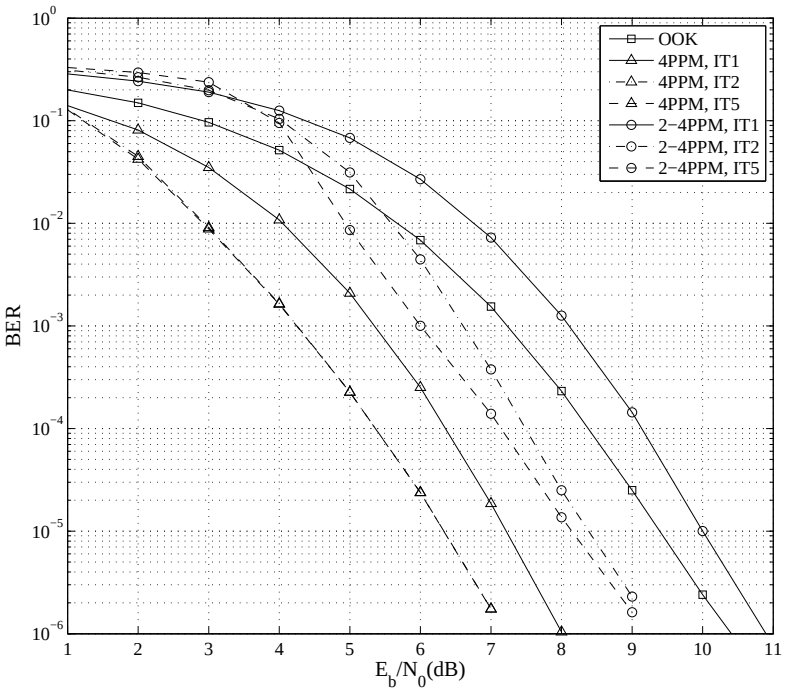

Figure 4. Comparison of different modulation schemes for AWGN channel. RSC $(1, 5/7)$ code, ITm denotes mth iteration.

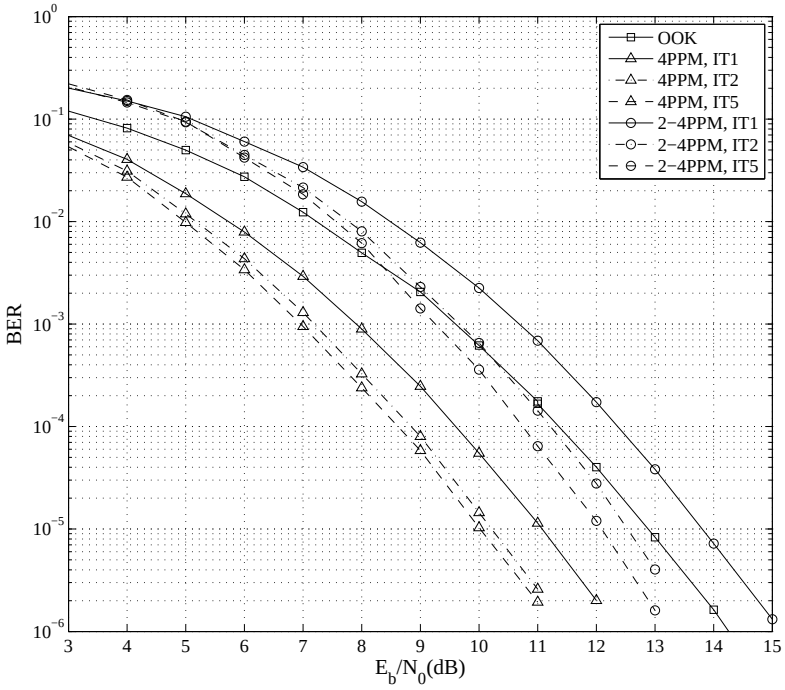

Figure 5. Comparison of different modulation schemes for the weak turbulence channel. RSC $(1, 5/7)$ code, ITm denotes mth iteration.

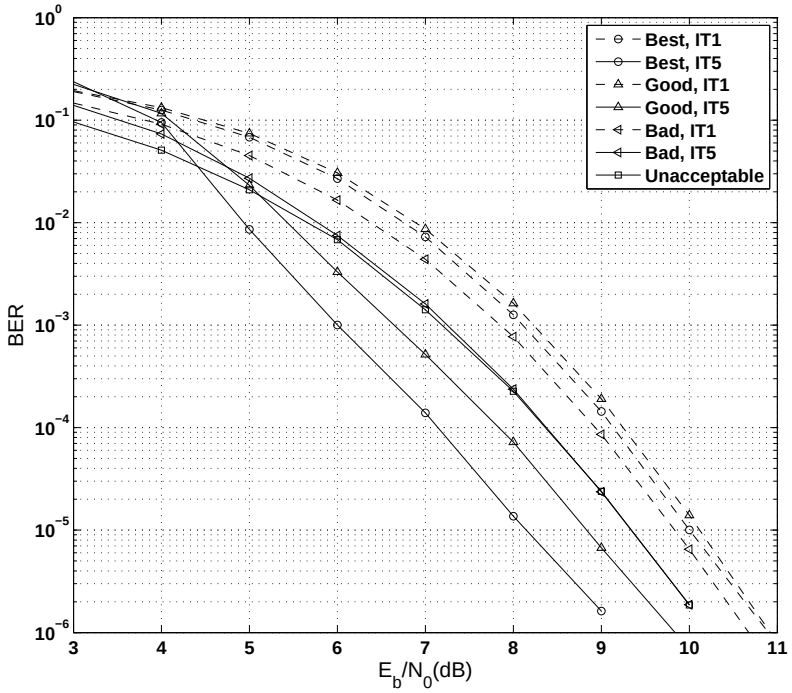

Figure 6. Performance of the iterative receiver for 2-4PPM modulation with $B = 2$ for different mappings for the AWGN channel. RSC $(1, 5/7)$ code, ITm denotes mth iteration.

6.2.2 Case of weak-turbulence channel

We have also compared the BER performances of different modulation schemes for the case of a weak turbulence channel in Fig. 5. The performance improvement by iterative method is again significant. For example, at BER= 10^{-5}, the SNR gain after full convergence is about 1.05 dB and 1.7 dB for the cases of 4PPM and 2-4PPM, respectively. Compared to the AWGN channel case, we notice that the full convergence is attained after five iterations for both modulation schemes.

6.3 Comparison of different bit-symbol mapping for 2-4PPM

We consider the cases of 2-4PPM for which we discussed the bit-symbol mapping in Subsection 5.1. Note that, in general, there is more correlation between the bit-level LLRs at the demapper output for MPPM, compared to the equivalent PPM scheme, and a larger interleaver should be used. We use an interleaver size of 4000 for the case of 2-4PPM.

We have shown in Fig. 6 the receiver BER performances for the four mappings already specified in Table 1, for the case of an AWGN channel. Firstly, consider the mapping "Best" whose performance wad illustrated in the previous subsection. It has the best performance after the receiver convergence as it has the largest d and d_1 (see Table 1 and Subsection 5.1). The best performance in the first iteration is obtained for the mapping "Unacceptable" for which we have the maximum d and d_2. Concerning the mappings "Good" and "Bad," which have the same d, better performance is obtained at the first iteration for the latter (which has a larger d_2), whereas after the convergence, a lower BER is achieved for the former (which has a larger d_1). For the case of weak turbulence channel, the same behavior is observed that are not shown here. Compared to the AWGN channel case, the SNR gain after full convergence is less significant, but still considerable.

6.3.1 Convergence analysis of the iterative receiver

We use the EXIT (EXtrinsic Information Transfer) charts[16, 17] to study the convergence of the receiver. Let us first present a brief introduction on this tool. EXIT charts are based on the flow of the extrinsic information

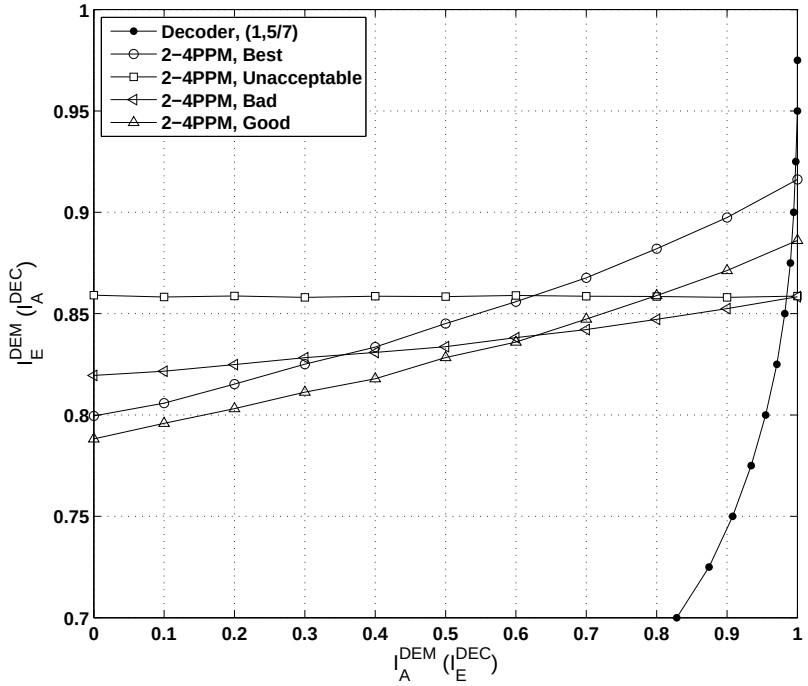

Figure 7. EXIT charts of the SOVA decoder and the demapper for the mappings in Tables 1 for 2-4PPM modulations at $E_b/N_0 = 8$ dB, AWGN channel.

exchanged between the SISO blocks in an iterative scheme. By this method, the LLRs input to a SISO block are assumed to be uncorrelated and to follow a Gaussian distribution. Denoting the *a priori* LLRs by ξ and their mean and variance by μ_ξ and σ_ξ^2, respectively, we furthermore assume that $\mu_\xi = \sigma_\xi^2/2$ corresponding to a bit 1, and $\mu_\xi = -\sigma_\xi^2/2$ corresponding to a bit 0.[16]

Let us denote by $I_{\rm A}$ ($._{\rm A}$ for *a priori*) and $I_{\rm E}$ ($._{\rm E}$ for extrinsic), the mutual information (MI) at the input and output of a SISO block, respectively. The EXIT chart is considered as the transfer function mapping the input information $I_{\rm A} \in [0,1]$ to the output information $I_{\rm E} \in [0,1]$. To obtain the EXIT curves, for each given $I_{\rm A}$, we generate at the input of a SISO block, Gaussian distributed *a priori* LLRs with the appropriate variance. The MI $I_{\rm E}$ at the output of the module is then calculated by histogram estimation. The behavior of the iterative detector is determined by associating $I_{\rm E}^{\rm DEM} \Rightarrow I_A^{\rm DEC}$, and inversely, $I_{\rm E}^{\rm DEC} \Rightarrow I_{\rm A}^{\rm DEM}$, where the superscripts $.^{\rm DEM}$ and $.^{\rm DEC}$ refer to the demapper and the channel decoder, respectively.

We have shown in Fig. 7 the EXIT chart of the SOVA decoder for RSC $(1, 5/7)$, as well as those of the demapper for different mappings at $E_b/N_0 = 8$ dB for the case of an AWGN channel. Note that the final BER depends on the intersection point of the EXIT curves of the demapper and the decoder. The closer the corresponding $I_{\rm E}^{\rm DEC}$ is to one, the lower the BER. We notice that, for instance, in the absence of *a priori* MI, i.e., at the first iteration, the demapper for "Bad" provides a higher output MI than for "Best." However, for relatively high *a priori* MI ($I_{\rm A}^{\rm DEM} > 0.35$) , we have a larger demapper output MI for the mapping "Best." The intersection with the EXIT curve of the decoder is at a higher $I_{\rm E}^{\rm DEC}$ and, as a result, the final BER is lower. This illustrates the famous trade-off between earlier turbo cliff and lower BER floor. We also notice that for "Unacceptable" the demapper EXIT curve is horizontal and no evolution of MI is achieved through iterations.

Note that the assumption of uncorrelated Gaussian *a priori* LLRs is not perfectly satisfied in practice. As a result, EXIT charts do not predict the convergence behavior of the receiver exactly. In other words, the obtained trajectory provides an asymptotic description of the receiver convergence.

7. CONCLUSIONS

We considered in this paper the use of binary convolutional coding with iterative detection for the case of MPPM modulation. We showed that a significant performance improvement is obtained by using the iterative scheme. We discussed the impact of bit-symbol mapping on the channel capacity as well as on the performance of the iterative receiver. In particular, we addressed a design rule to obtain optimal mappings adapted to the proposed iterative detection scheme. In order to optimize the mapping, first we choose symbol-sets which maximize the average Hamming distance d between different MPPM symbols. Then we choose among these sets, one that maximize in descending priority order d_1, d_2,..., d_B, where B is the number of bits per symbol and d_i is the average Hamming distance between symbols differing in i bits.

Acknowledgment

This work was supported in part by the French PACA (Provence-Alpes-Côte d'Azur) Regional Council.

REFERENCES

1. Chan, V. W. S., "Free-space optical communications," *J. Lightwave Technol.* **24**, 4750–4762 (Dec. 2006).
2. Andrews, L. C. and Phillips, R. L., [*Laser Beam Propagation through Random Media*], SPIE Press, Bellingham, Washington, second ed. (2005).
3. Xu, F., Khalighi, M. A., Caussé, P., and Bourennane, S., "Channel coding and time-diversity for optical wireless links," *Optics Express* **17**, 872–887 (Jan. 2009).
4. Xu, F., Khalighi, M. A., Caussé, P., and Bourennane, S., "Performance of coded time-diversity free-space optical links," *Queen's 24th Biennial Symposium on Communications (QSBC)* , 146–149 (June 2008). Kingston, Canada.
5. Xu, F., Khalighi, M.-A., and Bourennane, S., "Pulse position modulation for FSO systems: Capacity and channel coding," *ConTEL Conference* , 31–38 (June 2009). Zagreb, Croatia.
6. Khalighi, M.-A., Aitamer, N., Schwartz, N., and Bourennane, S., "Turbulence mitigation by aperture averaging in wireless optical systems," *ConTEL Conference* , 59–66 (June 2009). Zagreb, Croatia.
7. Wilson, S. G., Brandt-Pearce, M., Cao, Q. L., and Baedke, M., "Optical repetition MIMO transmission with multipulse PPM," *IEEE on Selected Areas in Communications* **23**, 1901–1910 (Sept. 2005).
8. Moision, B. and Hamkins, J., "Multipulse PPM on discrete memoryless channels," *IPN Progress Report* **42-160** (Feb. 2005).
9. Simon, M. K. and Vilnrotter, V. A., "Performance analysis and tradeoffs for dual-pulse PPM on optical communication channels with direct detection," *IEEE Transactions on Communications* **52**, 1969–1979 (Nov. 2004).
10. Moision, B. and Hamkins, J., "Deep-space optical communications downlink budget: modulation and coding," *IPN Progress Report* **42-154** (Aug. 2003).
11. Haas, S. M. and Shapiro, J. H., "Capacity of wireless optical communications," *IEEE on Selected Areas in Communications* **21**, 1346–1357 (Oct. 2003).
12. Moision, B. and Hamkins, J., "Coded modulation for the deep-space optical channel: serially concatenated pulse-position modulation," *IPN Progress Report* **42-161** (May 2005).
13. Barsoum, M. F., Moision, B., Fitz, M., Divsalar, D., and Hamkins, J., "Iterative coded pulse-position-modulation for deep-space optical communications," *Information Theory Workshop* , 66–71 (Sept. 2007).
14. S. ten Brink, "Designing iterative decoding schemes with the extrinsic information transfer charts," *AEÜ International Journal of Electronics and Communications* **54**, 389–398 (Nov. 2000).
15. Muhammad, N. S. and Speidel, J., "Joint optimization of signal constellation bit labeling for bit-interleaved coded modulation with iterative decoding," *IEEE Communications Letters* **9**, 775–777 (Sept. 2005).
16. S. ten Brink, "Convergence behavior of iteratively decoded parallel concatenated codes," *IEEE Transactions on Communications* **49**, 1727–1737 (Oct. 2001).
17. Tuchler, M., Koetter, R., and Singer, A. C., "Turbo equalization: principles and new results," *IEEE Transactions on Communications* **50**, 754–767 (May 2002).